FGF21-FGFR1 controls mitochondrial homeostasis in cardiomyocytes by modulating the degradation of OPA1

Yaling Han (✉ hanyaling@163.net)

General Hospital of Northern Theater Command   https://orcid.org/0000-0003-4569-6737

Bing Yan

Second Hospital of Jilin University   https://orcid.org/0000-0002-7821-5808

Zhu Mei

General Hospital of Northern Region

Yaohan Tang

General Hospital of Northern Theater Command

Haixu Song

General Hospital of Northern Theater Command

Hanlin Wu

General Hospital of Northern Theater Command

Xiaolin Zhang

General Hospital of Northern Theater Command

Chenghui Yan

General Hospital of Northern Theater Command   https://orcid.org/0000-0003-3409-8547

Abstract

Fibroblast growth factor 21 (FGF21) is a pleiotropic hormone, secreted mainly by the liver, considered as a major regulator of energy homeostasis. Recent research revealed that FGF21 could play an important role in cardiac pathological remodeling effects and preventing cardiomyopathy, but the underlying mechanism remained largely unknown. The aim of this study was to clarify the mechanism of FGF21 cardiac protective effects. We engineered FGF21 knock out mice, and the effects of FGF21 and its downstream mediators were subsequently elucidated using western blot, qRT-PCR, and mitochondrial morphological, functional analysis. FGF21 knock out mice resulted in cardiac dysfunction accompanied by a decline in global longitudinal strain (GLS) and ejection fraction (EF) which was independently of obesity. Mitochondrial quality, quantity and functions were abnormal accompanied with the decreased levels of optic atrophy-1 (OPA1) in FGF21 KO mice. In contrast to FGF21 knockdown, the cardiac specific overexpression of FGF21 can alleviate cardiac dysfunction caused by FGF21 deficiency. In vitro study FGF21 siRNA can deteriorate mitochondrial dynamics, functions impairment induced by $CoCl_2$. Both recombinant FGF21 and adeno virus mediated FGF21 overexpression can alleviate $CoCl_2$ induced mitochondrial impairment by restoring mitochondrial dynamics. FGF21 is essential for maintaining mitochondrial dynamics and functions in cardiomyocytes. FGF21, as an important target in regulating cardiomyocytes mitochondrial homeostasis under oxidative stress, will provide new therapeutic options for heart failure patients.

Introduction

FGF21 is well known as an endocrine hormone increase fat mobilization and increase insulin sensitive(1−4). FGF21 conduct its regulation of metabolic homeostasis mainly through FGFR1(5). Consider the closely association between metabolism and cardiovascular system, there are research investigated the cardiac effect of FGF21. The results show FGF21 could protect against hypertrophic cardiomyopathy(6−8) which is the early stage of cardiac dysfunction in mice model(9). But there are confusing results in clinical research, which is increased serum FGF21 in HFrEF patients and it is correlated with worsen outcomes(10, 11). Whether FGF21 has protect effect or harmful directly for cardiac function is still unknow.

Mitochondrial are important organelles that maintain cell energy production and other biological processes(12). They can adapt to a variety of endogenous and exogenous stimuli mainly through dynamic changing of fission and fusion,(13) so mitochondrial dynamics is a vital mechanism that protecting mitochondrial from damage(14). Damaged mitochondrial is closely associated with the cardiac dysfunction(15−17). OPA1 is dynamin like GTPase located in the inner mitochondrial membrane, that regulate mitochondrial fusion and maintain mitochondrial cristae structure(18,19). OPA1 also play an important role in maintain mitochondrial function by regulating respiratory supercomplexes assembly and modulating mitochondrial calcium uptake(20, 21).

To elucidate the effect of FGF21 on cardiac function we concentrated on what and how FGF21 effect cardiac function. In this study, we observed cardiac dysfunction in FGF21 KO mice, and found that FGF21 deficiency can cause sever mitochondrial damage both in vivo and in vitro. Both exogenous addition and endogenous overexpression could alleviate mitochondrial damage cause by $CoCl_2$ stimulation. Therefore, we further investigated the mechanism that FGF21 maintaining mitochondrial homeostasis and found that FGF21 could inhibition OPA1 degradation through activation of FGFR1 and increased FBXW11 degradation.

Results

FGF21 KO mice developed cardiac dysfunction before impaired metabolic state onset

To understand the mechanism of how FGF21 possesses beneficial effects on cardiovascular health, we conducted FGF21 KO mice (**Fig.S1 A-D**), and we closely monitored the metabolic baseline data and cardiac function of FGF21 KO mice. Unexpectedly, though FGF21 is a key regulator of metabolism, there are significant differences in cardiac diastolic function between FGF21 KO mice and their littermate in young age (16 weeks old) but not in blood sugar and body weight, as evidenced by comparable global longitudinal strain, longitudinal and radial strain time to peak (Fig. 1A-C, **and** Fig.S1E-1H). In young age FGF21 KO heart also found mild hypertrophic features and increased cardiac fibrosis (Fig. 1D, 1E). Meanwhile, the cardiac impaired marker BNP, hypertrophy marker MYH7, and fibrosis marker was also increased (Fig. 1F). Although eject fraction has no significant impairment in young age FGF21 KO mice, severe systolic dysfunction developed after 22 weeks old (**Fig. S2A, B**). These results suggest that FGF21 play a key role in maintain cardiac function.

FGF21 KO mice OPA1 degradation increased, and mitochondrial structure was severely damaged

To investigate how FGF21 deficiency mediates the cardiac dysfunction, we next examined the morphological and function of heart tissue in FGF21 KO mice and their littermates. TEM analysis demonstrated that sarcomere arrangement and mitochondrial morphological were disrupted in FGF21 KO mice (Fig. 2A). The average cross-sectional area of individual mitochondrial, mitochondrial perimeter, and mitochondrial area were significantly reduced in FGF21 KO mice (Fig. 2B). A 5-grade scoring system analysis showed that FGF21 deficiency induced severe damage in mitochondrial morphology with inflation, warped membranes, irregularities, and absence of cristae (Fig. 2C,2D, **and Fig.S3A**).

To elucidate the mechanism of mitochondrial damage, we further investigated mitochondrial dynamic related protein, mitochondrial genesis associated protein, and mitophagy indicator. There was no difference of mitochondrial genesis protein but in mitochondrial dynamic related protein OPA1 was significantly decreased, and mitophagy related protein PINK and PARKIN were significantly increased in

FGF21 KO mice (Fig. 2E, 2F). We further investigated the mRNA levels of related protein, there are no differences between FGF21 KO mice and their littermates (Fig. 2G). To further investigate whether the OPA1 decreased impact the mitochondrial dynamics in cardiomyocytes, we use Mitotracker staining to evaluate the mitochondrial morphology in isolated adult cardiomyocytes. As expected, the FGF21 KO isolated adult cardiomyocytes mitochondrial is characterized by increased splitting and swelling (Fig. 2H-J). These results suggest that FGF21 deficiency may cause increased OPA1 degradation and mitochondrial damage.

Restoration of cardiac FGF21 reverses impaired cardiac function in FGF21 KO mice

To confirm FGF21 has cardiac-specific effect on protecting mitochondrial damage, an adeno-associated virus carrying a TNT-GFP promoter (AAV-TNT-GFP) was used to monitor FGF21 cardiac-specific overexpression in FGF21 KO mice (Fig. 3A, **Fig.S4A**). FGF21 cardiac-specific overexpression had no effect on metabolic status (**Fig.S4B, C**), but obviously improved the cardiac dysfunction caused by FGF21 deficiency 16 weeks after injection, as shown by the EF%, GLS% (Fig. 3B, C). Consistently, FGF21 cardiac-specific overexpression reversed cardiac hypertrophy and fibrosis caused by FGF21 deficiency (Fig. 3D, 3E). Cardiac impaired marker BNP, hypertrophy marker MYH7, and fibrosis marker was also decreased in FGF21 cardiac-specific overexpression mice (Fig. 3F). Western blotting identified that OPA1 expression was increased and mitophagy is inhibited in FGF21 cardiac-specific overexpression mice (Fig. 3G, H).

Furthermore, Mitotracker staining of the FGF21 KO mice mitochondrial in isolated adult cardiomyocytes reveal that FGF21 cardiac-specific overexpression reversed increased mitochondrial splitting and swelling (Fig. 3I-3K). These results demonstrated that FGF21 cardiac-specific overexpression could reverse cardiac dysfunction caused by FGF21 deficiency.

FGF21 deficiency caused OPA1 degradation and abnormal mitochondrial structure and function in vitro

To further explore the effect of FGF21 in maintaining mitochondrial homeostasis, we transfected cardiomyocytes with siFGF21. As expected FGF21 deficiency caused OPA1 degradation (Fig. 4A). Mitotracker staining showed increased fission with decreased mitochondrial network branches and branch length in cardiomyocytes with siFGF21 transfection (Fig. 4B, C). To validate whether FGF21 deficiency could affect mitochondrial oxidative phosphorylation, we used an extracellular flux analyzer to assess mitochondrial function in cardiomyocytes. FGF21 deficiency cardiomyocytes had similar levels of basal respiration and proton leak compared with normal cardiomyocytes, but the maximal respiratory capacity and spare capacity were markedly reduced (Fig. 4E-G).

Overexpression of FGF21 has no effect on physiological mitochondrial function

As the role of FGF21 in maintaining mitochondrial homeostasis was confirmed, we explored whether FGF21 could regulates mitochondrial function under physiological condition. We further evaluated the

mitochondrial dynamics and function after given recombination FGF21 or adFGF21. Under physiological status recombination FGF21 or AdFGF21 has no effect on mitochondrial dynamics and function (FigS5A-J).

In vitro both autocrine and exogenous FGF21 could defenses mitochondrial damage under stressing

To further explored whether FGF21 could defenses mitochondrial damage under stressing conditions, we use different stimulators to detect the expression of FGF21 and OPA1 in cardiomyocytes. As shown in (Fig.S6 A-F), $CoCl_2$ can active Hif1-a expression, and inhibited FGF21 and OPA1 expression in dose- and time-dependent manner. Moreover, $CoCl_2$ stimulation also cause increased mitochondrial fission and impairment of mitochondrial function (Fig.S6 G-K).

Under $CoCl_2$ stimulation, recombination FGF21 and adFGF21 could both restore OPA1 levels (Fig. 5A-D). Then we further investigated the mitochondrial morphology, given recombination FGF21or adFGF21 both can restore mitochondrial dynamic, decrease fission, also could increase fusion and branches forming, under $CoCl_2$ stimulation (Fig. 5E-H). As expected, FGF21 overexpression dramatically improved both spare and maximal respiratory capacity but did not affect basal respiration, H^+ leak, or respiration attributed to basal F1/F0 ATP synthase activity (Fig. 5I-K).

FGF21 is an endocrine protein, mainly secreted by liver but cardiomyocyte could also synthesis and secrete FGF21. As shown in (Fig.S7A), the adFGF21 cardiomyocytes culture supernatant was with significantly high FGF21 levels. When given Monensin, which is an intracellular protein transport blocker, the high FGF21 levels in the adFGF21 cardiomyocytes culture supernatant was decreased. In contrast, Monensin administration ignored the rescue of adFGF21 on mitochondrial damage induced by $CoCl_2$ (Fig.S7B-7G).

Inhibition of FGFR1 impairs the mitochondrial protected effect of FGF21 under CoCl $_2$ stimulation in vitro

As previous study(22, 23), FGFR1 and FGFR3 are the mainly expressed FGF21 receptors on heart (Fig. S8A). To determine FGF21 to exert its effect on heart through FGFR1 or FGFR3. First, we transfected cardiomyocytes with siFGFR1 or siFGFR3 respectively. Only FGFR1 deficiency could inhibitor OPA1 restoration caused both by recombination FGF21 and endogenous FGF21 under $CoCl_2$ stimulation (Fig. S8B, C, Fig. 6A-6D). We next sought to validate whether FGF21 exert its effect on mitochondrial through activating FGFR1. As expected, both endogenous or exogenous FGF21 couldn't prevent OPA1 degradation in FGFR1 absence cardiomyocytes (Fig. 6A-D) and Mitotracker staining shows in FGFR1 absent cardiomyocytes FGF21 couldn't restore decreased mitochondrial fusion caused by $CoCl_2$ (Fig. 6E-H). We also test the mitochondrial oxidative phosphorylation in these FGFR1 absent cardiomyocytes. Upregulation of spare and maximal respiratory capacity by FGF21 in $CoCl_2$ stimulated cardiomyocytes was absent (Fig. 6I-N). These results suggest that activation of FGFR1 is required for FGF21-mediated mitochondrial protected effect.

OPA1 mediated mitochondrial damage caused by FGF21 deficiency or under CoCl$_2$ stimulation

To determine whether the regulating of OPA1 plays an important role in FGF21-induced the mitochondrial homeostasis. We overexpressed the OPA1 by transfected with OPA1 plasmid in FGF21 knock down cardiomyocytes or cardiomyocytes under CoCl$_2$ stimulation and investigated the mitochondrial morphological change. As shown in (Fig. 7A-D), overexpression of OPA1 could restore mitochondrial dynamics with increased mitochondrial network branches and branch length in FGF21 knock down cardiomyocytes or cardiomyocytes under CoCl$_2$ stimulation. Overexpression of OPA1 could also restore the mitochondrial function and reduce the mitophagy which cause by FGF21 deficiency or CoCl$_2$ stimulation (Fig. 7E-I). These results suggest that FGF21 maintain mitochondrial homeostasis through regulating OPA1.

FGFR1 regulate OPA1 degradation through E3 ligase FBXW11

Due to FGF21 deficiency and overexpression of FGF21 has no effect on mRNA levels of OPA1, the possible OPA1 degradation modulators were identified in cardiomyocytes. Firstly, we found that MG132 could inhibitor OPA1 degradation in time-dependent manner (Fig. 8A, B). In contrast, FGF21 administration remarkably reduced the OPA1 degradation in cardiomyocytes under CHX stimulation (Fig. 8C, D). These results indicate that FGF21 regulated the degradation of OPA1.

To determine the E3 ligase binding to OPA1, we use UbiBrowser to predict potential OPA1 E3 ligase (Fig.S9A). We evaluated several E3 ligases expression, FBXW11 was detected to obvious increase in FGF21 KO mice heart compared to that in littermate mice in protein level but not in mRNA level (Fig. 8E, F, and Fig. S9B). Further with CoCl$_2$ stimulation, FBXW11 remarkably increased in cardiomyocytes associated with the reduction of OPA1 and FGF21 (Fig. 8G, H). As expected, silence of FGF21 increased the FBXW11 expression, and overexpression of FGF21 decreased the FBXW11 expression (Fig. 8I-L). Moreover, the OPA1 degradation increased after overexpression of FBXW11, and transfection of siRNAs targeting FBXW11 reduced OPA1 degradation in cardiomyocytes caused by CoCl$_2$ stimulation (Fig. 8M-P), further suggesting that OPA1 is a possible physiologic substrate of FBXW11. To confirm the result, we detected the interaction between FBXW11 and OPA1 by IP assay. As shown in (Fig. 8Q, R) overexpression of FBXW11 increased the ubiquitin of OPA1.

Because FGF21 exert its effect mainly through activation of FGFR1 which is tyrosine kinase receptor, we continued to investigate whether FGFR1 could interact with FBXW11. In transfected siFGFR1 cardiomyocytes we found increase FBXW11 (Fig.S10A, B). Next, we further constructed FGFR1 plasmid then we transfected FGFR1 after evaluated the phosphorylation levels of FBXW11, we found out increased FBXW11 degradation (Fig.S10C, D). Collectively, these results support the notion that OPA1 is a degradation substrate of the FBXW11 and FGFR1 activation could increase FBXW11 degradation.

Discussion

In the present study, we demonstrated that cardiomyocytes mitochondrial is a direct target of autocrine and endocrine FGF21, as summarized in **Fig. S10E**. The absence of FGF21 is associated with damaged mitochondrial structure and function both *in vitro* and *in vivo*, which is caused by increase degradation of OPA1. And endogenous or exogenous FGF21 both can protect cardiomyocytes mitochondrial from stressing stimulation *in vitro* and *in vivo*. We also confirmed that the degradation of OPA1 is meditated by FGFR1 rather than FGFR3, and the inhibition of OPA1 degradation is mainly by increase FBXW11 degradation, which is an E3 ligase of OPA1.

FGF21 was discovered as a key regulator of metabolism status, that regulate lipid and glucose metabolism(24), and has a role in many mitochondrial related diseases(25–27). And there are many reports about the cardiovascular beneficial(28). But the mechanism of how FGF21 exert benefit effect on cardiac is still not quite clear. There is previous study found that FGF21 could protect cardiac function from cardiac hypertrophy(6), and significant cardioprotective effective of FGF21 in a mouse model of experiment MI(8, 29). And there are reports about FGF21 could protect diabetic cardiomyopathy formation by inhibition ROS(30, 31). Although there are reports about FGF21 has effect on muscle and live mitochondrial status(27), and serum FGF21 is a biomarker of mitochondrial(25, 26), but there is no report about whether FGF21 has effect on cardiomyocytes mitochondrial morphology or function. We found in FGF21 KO mice there are severely damaged mitochondrial accompany with increased mitophagy. Moreover, we found that FGF21 also play a key role in maintaining mitochondrial normal function. In summary, our present results are consistent with the heart being a direct target of FGF21 and it plays a key role in maintaining mitochondrial homeostasis.

OPA1 is emerging as a critical regulator to balance mitochondrial fusion and fission(32, 33), and normal mitochondrial dynamics is important for cardiac metabolism. OPA1 is needed for PTP-induced mitochondrial swelling and mitochondrial respiratory supercomplexes assembly and oxidative phosphorylation(34). In our present study we found that in FGF21 KO mice OPA1 is significantly decreased, and in vitro we found that FGF21 could regulate OPA1 degradation. There is no report about the association about FGF21 and OPA1. In previous studies reports that FGF21 could reduce the ROS production and protect mitochondrial from damage. Our results found a new mechanism how FGF21 regulated mitochondrial homeostasis. We further investigated the degradation of OPA1 and found that FBXW11 exert the degradation of OPA1, which is inhibited by FGF21. In vitro study we found that $CoCl_2$ stressing and FGF21 deficiency both could increase FBXW11 level which is predicted as OPA1 E3 ligase. And overexpression FBXW11 could downregulation OPA1 and knock down FBXW11 could upregulation OPA1. These results in our present study shows that FGF21 could regulate OPA1 degradation through FBXW11, which give much more detail about how FGF21 regulate OPA1.

In previous studies it is well established that cardiac could also secret FGF21 through the secretion is much lesser than liver or white adipose tissue(35–37). For cardiac the FGF21 that works on cardiomyocytes could be FGF21 came from circulation or from cardiac itself. So, in our study we prove

that FGF21 could exert its effect through both endocrine and autocrine, by added exogenous recombination FGF21 or overexpression by using AdFGF21. Both of two ways could have cardiac protect effect. Then we through the knock down FGFR1 or FGFR3 to confirm which receptor mediated the cardiac protected effect of FGF21. Knock down FGFR1 could significantly diminish the protected effects of FGF21, and overexpression could increase the activation of FGFR1 and inhibition of OPA1 degradation and downregulation of FBXW11. These results reveal that activation of FGFR1 could increase FBXW11 degradation and inhibition OPA1 degradation.

Collectively, the finding reported in this study indicates that FGF21 is needed for maintaining mitochondrial homeostasis and under stressing stimulation addition FGF21 restore the mitochondrial damage. Reveal that FGF21-FGFR1-OPA1 axis could provide potential therapeutic targets for cardiac dysfunction.

Materials And Methods

Animals

FGF21 knockout mice in C57BL/6J background were generated as previously described(38). All animals were housed in temperature-controlled cages with a 12-h light dark cycle and provided free access to food and water. All animal study procedures were approved by the Cardiovascular Research Institute and the Department of Cardiology of the General Hospital of Northern Theater Command and conformed to the National Institutes of Health (NIH) Guide for the Care and Use of Laboratory Animals. Adeno-associated virus AAV-TNT-GFP-FGF21 and control virus AAV-TNT-GFP from HanbioTech (Shanghai, China) were injected into the tail of mice.

Glucose tolerance tests

For glucose tolerance tests, fasting blood glucose levels from tail blood were measured after a 16-h fast, using the glucometer. Mice were then given an intraperitoneal injection of glucose at a dose of 1.5 g per kg body weight. We measured blood glucose at basal, 30, 60, 90, and 120 minutes from tail blood using the glucometer.

Echocardiography measurements

Echocardiography was performed using the Vevo 2100 Ultrasound System (FUJIFILM, Visual Sonics). Mouse cardiac echocardiography measurements were performed under 1% isoflurane anesthesia to detect cardiac function, and mouse cardiac function was detected using a 30-MHz high-frequency scan head as previously described. Parasternal long-axis images were acquired in B-mode with appropriate positioning of the scan head and the maximum LV length identified. In this view, the M-mode cursor was positioned perpendicular to the maximum LV dimension in end-diastole and systole, and M-mode images were obtained for measuring wall thickness and chamber dimensions. Speckle tracking-based strain analyses were performed on parasternal long-axis B-mode loops using the Vevo Strain Software (Vevo LAB) as previously described(39).

Transmission electron microscopy (TEM)

First, fresh hearts removed from mice or freshly collected cardiomyocytes were perfused with an

electron microscope fixing solution (4% paraformaldehyde and 1% glutaraldehyde in 0.1 mol/L sodium cacodylate buffer, pH 7.4, and 4% sucrose). Then, 2% osmium tetroxide and 0.8% potassium ferrocyanide in a 0.1 mol/L sodium cacodylate buffer were employed to pre-fix for 2 h and odium cacodylate buffer was used to wash three times. The samples were dehydrated using a density gradient of alcohol and acetone. Finally, the samples were cut into 60–80 nm ultrathin slices, dyed, and dried overnight at room temperature. The sections were imaged and analyzed using an H-7800 TEM (Hitachi High-Technologies Europe GmbH, Krefeld, Germany). The average number of mitochondria from each sample was determined from a randomly selected pool of 15 to 20 fields under each condition. Mitochondrial appearance in EM images was determined by using a five-grade scoring system as previously described(40). Number of mitochondrial, average mitochondria cross-sectional area, cristae number were determined as previously described with Image J.(41)

Cardiac perfusion

LV cardiomyocytes are isolated enzymatically using a Langendorff perfusion system as previously described(42). Briefly, Langendorff perfusion system was set up firstly, then mice were anesthetized and

hearts were transferred to a 60-mm dish and wash it with NT solution. Mount the aorta onto the Langendorff perfusion cannula, and then firmly ligate the aorta onto the cannula. Then switch the perfusate to A solution (Tyrode solution + 10 mM Taurine, 1 mg/mL BSA) to stop the heartbeat and wash the blood. Next, switch the perfusate to E isolation solution (A solution + 0.6 mg/mL type II collagenase) for enzyme digestion for 12 min. Finally, place the heart in a 35-mm dish containing KB solution and cut off the LV tissue into small pieces. Centrifuge at 150 x g for 30 s and discard the supernatant. Re-suspend the myocytes in 10 mL KB solution, free settle for 6 min, discard the supernatant, and re-suspend the pellet in KB solution for further treatment.

Histological and immunofluorescent study

Heart tissues were dissected out and fixed with 4% paraformaldehyde. 5µm cross-sections from the fixed hearts were stained with Sirius red according to the manufacture's protocol. For Mitotracker staining, the fresh cardiomyocytes were fixed in 10% formalin for 30min at room temperature and then washed 3 times in PBS. The fixed sections were then incubated with 4µM Mitotracker dye (Thermo Fisher Scientific) for 30min. After washing, sections were stained with 4',6'-diamidino-2-phenylindole (DAPI, Thermo Fisher Scientific) and covered with glass coverslips. All slides were examined under the Zeiss colocalization microscope. Mitochondrial network morphology analysis was performed with ImageJ as previously described(41).

Cell culture

Primary mouse cardiomyocytes were prepared from neonatal mice (days 0–2), digested with 0.2% collagenase II, neutralized with two times the volume of serum, and filtered with a 100 μm screen. Cardiomyocytes were then cultured in H-DMEM supplemented with 20% FBS, penicillin (100 U/mL),

and streptomycin (100 μg/mL) at 37°C with 5% CO_2 and 95% air. HL-1 cells were purchased from ATCC (Manassas, VA). The cells were then divided into different groups according to the experiment, as follows: adenovirus-loaded GFP or FGF21 (OBiO Technology, Shanghai, China), si-NC, si-FGF21, siFGFR1 and si-FBXW11 (RIBOBIO, Guangzhou, China).

Gene silencing and adenovirus infection

Briefly, cardiomyocytes were transfected with si-FGF21, si-FGFR1, si-FBXW11 (RIBOBIO, Guangzhou, China) using RNAiMAX (Life Technologies, Carlsbad, CA). For overexpression of FGF21, adenovirus encoding FGF21 (OBiO Technology, Shanghai, China) was used to transfect primary neonatal mouse cardiomyocytes and HL-1 cells.

Western blotting

First, protein lysates were centrifuged at 12,000 × g at 4°C for 15 min, prepared with loading buffer, and boiled for 5 min. Then, they were electrophoresed with 10% SDS and transferred onto polyvinylidene fluoride membranes (Merck, Millipore). After blocking with 5% defatted milk for 1 h, membranes were incubated with primary antibodies overnight at 4°C. Membranes were then incubated with horseradish peroxidase-conjugated secondary antibodies for 2 h at room temperature. The target proteins signal was detected using Amersham Imager 680 (GE, USA). Expression quantification was calculated with ImageJ. Detailed information for primary antibodies are listed in Supplementary Table S1.

Real-time quantitative PCR

Total mRNA was extracted by the Trizol Reagent method (Thermo Fisher Scientific), and complementary DNA was synthesized from 500ng total RNA by reverse transcription with Prime Script RT reagent kit (Takara) with random hexamer primers. Quantitative real-time PCR amplification was performed using SYBR Green (Takara), and GAPDH gene expression was used for normalization. Detailed primers are listed in Supplementary Table S2.

Seahorse XF Cell Mito Stress Test

HL-1 cardiomyocytes after treatment were seeded in laminin-coated microplates, and culture for 24–48 hours before measure the oxygen consumption rate (OCR). The measure of OCR in the Seahorses biosciences XF96 extracellular flux analyzer (Agilent, USA) following the standard procedures as previously described.

Statistical analysis

All data were analyzed using GraphPad Prism 8 software and are shown as the mean ± SEM. In our study, t-tests and one-way analyses of variance were employed to evaluate statistical significance. Statistical

significance was set at P < 0.05.

Declarations

CONFLICT OF INTEREST

The authors declare that the research was conducted in the absence of any commercial or financial relationships that could be construed as a potential conflict of interest.

AUTHOR CONTRIBUTIONS

BY conducted the research, BY and XZ wrote the manuscript, ZM, YT, and HS contributed to methodology, ZM and HW participated in data analysis, YLH and CHY designed the research and directed the study. All authors read and approved the final paper.

ETHICS STATEMENT

All experimental procedures in this study were approved by the Cardiovascular Research Institute and the Department of Cardiology of the General Hospital.

DATA AVAILABILITY STATEMENT

The data and material that support the findings of this study are available from the corresponding author upon reasonable request.

References

1. Geng L, Lam KSL, Xu A. The therapeutic potential of FGF21 in metabolic diseases: from bench to clinic. Nat Rev Endocrinol. 2020 Nov 6;16(11):654–67.
2. Fisher FM, Chui PC, Antonellis PJ, Bina HA, Kharitonenkov A, Flier JS, et al. Obesity is a fibroblast growth factor 21 (FGF21)-resistant state. Diabetes. 2010;59(11):2781–9.
3. Véniant MM, Hale C, Helmering J, Chen MM, Stanislaus S, Busby J, et al. FGF21 promotes metabolic homeostasis via white adipose and leptin in mice. PLoS One. 2012;7(7).

4. Panaro BL, Coppage AL, Beaudry JL, Varin EM, Kaur K, Lai JH, et al. Fibroblast activation protein is dispensable for control of glucose homeostasis and body weight in mice. Mol Metab [Internet]. 2019;19(November 2018):65–74. Available from: https://doi.org/10.1016/j.molmet.2018.10.011

5. Dolegowska K, Marchelek-Mysliwiec M, Nowosiad-Magda M, Slawinski M, Dolegowska B. FGF19 subfamily members: FGF19 and FGF21. J Physiol Biochem. 2019;75(2):229–40.

6. Planavila A, Redondo I, Hondares E, Vinciguerra M, Munts C, Iglesias R, et al. Fibroblast growth factor 21 protects against cardiac hypertrophy in mice. Nat Commun. 2013;4(May 2013).

7. Ruan CC, Kong LR, Chen XH, Ma Y, Pan XX, Zhang ZB, et al. A2A Receptor Activation Attenuates Hypertensive Cardiac Remodeling via Promoting Brown Adipose Tissue-Derived FGF21. Cell Metab. 2018 Sep 4;28(3):476-489.e5.

8. Joki Y, Ohashi K, Yuasa D, Shibata R, Ito M, Matsuo K, et al. FGF21 attenuates pathological myocardial remodeling following myocardial infarction through the adiponectin-dependent mechanism. Biochem Biophys Res Commun. 2015 May 30;459(1):124–30.

9. Nakamura M, Sadoshima J. Mechanisms of physiological and pathological cardiac hypertrophy. Nat Rev Cardiol [Internet]. 2018;15(7):387–407. Available from: http://dx.doi.org/10.1038/s41569-018-0007-y

10. Gu L, Jiang W, Zheng R, Yao Y, Ma G. Fibroblast Growth Factor 21 Correlates with the Prognosis of Dilated Cardiomyopathy. Cardiology (Switzerland). 2020;

11. Fan L, Gu L, Yao Y, Ma G. Elevated Serum Fibroblast Growth Factor 21 Is Relevant to Heart Failure Patients with Reduced Ejection Fraction. Comput Math Methods Med. 2022 Jan 11;2022:1–6.

12. Sorrentino V, Menzies KJ, Auwerx J. Repairing Mitochondrial Dysfunction in Disease. Annu Rev Pharmacol Toxicol [Internet]. 2017; Available from: https://doi.org/10.1146/annurev-pharmtox-

13. Gao S, Hu J. Mitochondrial Fusion: The Machineries In and Out. Vol. 31, Trends in Cell Biology. Elsevier Ltd; 2021. p. 62–74.

14. Dorn GW. Mitochondrial dynamism and heart disease: changing shape and shaping change. EMBO Mol Med. 2015 Jul;7(7):865–77.

15. Bravo-San Pedro JM, Kroemer G, Galluzzi L. Autophagy and Mitophagy in Cardiovascular Disease. Vol. 120, Circulation Research. Lippincott Williams and Wilkins; 2017. p. 1812–24.

16. Kang PM, Haunstetter A, Aoki H, Usheva A, Izumo S. Morphological and Molecular Characterization of Adult Cardiomyocyte Apoptosis During Hypoxia and Reoxygenation [Internet]. 2000. Available from: http://www.circresaha.org

17. Dey S, DeMazumder D, Sidor A, Brian Foster D, O'Rourke B. Mitochondrial ROS drive sudden cardiac death and chronic proteome remodeling in heart failure. Circ Res. 2018;123(3):356–71.

18. Ishihara N, Fujita Y, Oka T, Mihara K. Regulation of mitochondrial morphology through proteolytic cleavage of OPA1. EMBO Journal. 2006 Jul 12;25(13):2966–77.

19. Yu C, Zhao J, Yan L, Qi Y, Guo X, Lou Z, et al. Structural insights into G domain dimerization and pathogenic mutation of OPA1. Journal of Cell Biology. 2020;219(7).

20. Jang S, Javadov S. OPA1 regulates respiratory supercomplexes assembly: The role of mitochondrial swelling. Mitochondrion. 2020 Mar 1;51:30–9.

21. Wai T, García-Prieto J, Baker MJ, Merkwirth C, Benit P, Rustin P, et al. Imbalanced OPA1 processing and mitochondrial fragmentation cause heart failure in mice. Science (1979). 2015 Dec 4;350(6265).

22. Hughes SE. Differential expression of the fibroblast growth factor receptor (FGFR) multigene family in normal human adult tissues. J Histochem Cytochem [Internet]. 1997 [cited 2022 Oct 21];45(7):1005–19. Available from: https://pubmed.ncbi.nlm.nih.gov/9212826/

23. Ahmad I, Iwata T, Leung HY. Mechanisms of FGFR-mediated carcinogenesis. Biochimica et Biophysica Acta (BBA) - Molecular Cell Research. 2012 Apr;1823(4):850–60.

24. Lewis JE, Ebling FJP, Samms RJ, Tsintzas K. Going Back to the Biology of FGF21: New Insights. Trends in Endocrinology & Metabolism. 2019 Aug;30(8):491–504.

25. Huddar A, Govindaraj P, Chiplunkar S, Deepha S, Jessiena Ponmalar JN, Philip M, et al. Serum fibroblast growth factor 21 and growth differentiation factor 15: Two sensitive biomarkers in the diagnosis of mitochondrial disorders. Mitochondrion. 2021 Sep 1;60:170–7.

26. Lehtonen JM, Forsström S, Viscomi C, Zeviani M, Moraes C, Nakada K, et al. Mitochondrial myopathy biomarker Fibroblast growth factor 21 is induced by muscle mtDNA instability and translation defects. Mitochondrion. 2015 Sep;24:S45–6.

27. Li B, Liu L. Fibroblast growth factor 21, a stress regulator, inhibits Drp1 activation to alleviate skeletal muscle ischemia/reperfusion injury. Lab Invest [Internet]. 2022 Sep 1 [cited 2022 Oct 22];102(9):979–88. Available from: https://pubmed.ncbi.nlm.nih.gov/35488034/

28. Kliewer SA, Mangelsdorf DJ. A Dozen Years of Discovery: Insights into the Physiology and Pharmacology of FGF21. Vol. 29, Cell Metabolism. Cell Press; 2019. p. 246–53.

29. Ma Y, Kuang Y, Bo W, Liang Q, Zhu W, Cai M, et al. Exercise Training Alleviates Cardiac Fibrosis through Increasing Fibroblast Growth Factor 21 and Regulating TGF-β1-Smad2/3-MMP2/9 Signaling in Mice with Myocardial Infarction. Int J Mol Sci [Internet]. 2021 Nov 1 [cited 2022 Oct 22];22(22). Available from: https://pubmed.ncbi.nlm.nih.gov/34830222/

30. Planavila A, Redondo-Angulo I, Ribas F, Garrabou G, Casademont J, Giralt M, et al. Fibroblast growth factor 21 protects the heart from oxidative stress. Cardiovasc Res. 2015 Apr 1;106(1):19–31.

31. Wu F, Wang B, Zhang S, Shi L, Wang Y, Xiong R, et al. FGF21 ameliorates diabetic cardiomyopathy by activating the AMPK-paraoxonase 1 signaling axis in mice. Clin Sci. 2017 Aug 1;131(15):1877–93.

32. Li X, Li H, Xu Z, Ma C, Wang T, You W, et al. Ischemia-induced cleavage of OPA1 at S1 site aggravates mitochondrial fragmentation and reperfusion injury in neurons. Cell Death Dis. 2022 Apr 1;13(4).

33. Anderson CJ, Kahl A, Fruitman H, Qian L, Zhou P, Manfredi G, et al. Prohibitin levels regulate OMA1 activity and turnover in neurons. Cell Death Differ. 2020 Jun 1;27(6):1896–906.

34. Cartes-Saavedra B, Macuada J, Lagos D, Arancibia D, Andrés ME, Yu-Wai-Man P, et al. OPA1 Modulates Mitochondrial Ca2+ Uptake Through ER-Mitochondria Coupling. Front Cell Dev Biol. 2022 Jan 3;9.

35. Liu L, Pasumarthi KBS, Padua RR, Massaeli H, Fandrich RR, Pierce GN, et al. Adult cardiomyocytes express functional high-affinity receptors for basic fibroblast growth factor. Am J Physiol [Internet]. 1995 [cited 2022 Oct 21];268(5 Pt 2). Available from: https://pubmed.ncbi.nlm.nih.gov/7771542/

36. Giralt M, Gavaldà-Navarro A, Villarroya F. Fibroblast growth factor-21, energy balance and obesity. Mol Cell Endocrinol. 2015 Dec;418:66–73.

37. Planavila A, Redondo-Angulo I, Villarroya F. FGF21 and Cardiac Physiopathology. Vol. 6, Frontiers in Endocrinology. Frontiers Media S.A.; 2015.

38. Hotta Y, Nakamura H, Konishi M, Murata Y, Takagi H, Matsumura S, et al. Fibroblast growth factor 21 regulates lipolysis in white adipose tissue but is not required for ketogenesis and triglyceride clearance in liver. Endocrinology. 2009 Oct;150(10):4625–33.

39. de Lucia C, Wallner M, Eaton DM, Zhao H, Houser SR, Koch WJ. Echocardiographic Strain Analysis for the Early Detection of Left Ventricular Systolic/Diastolic Dysfunction and Dyssynchrony in a Mouse Model of Physiological Aging. Journals of Gerontology - Series A Biological Sciences and Medical Sciences. 2019 Mar 14;74(4):455–61.

40. Eisner V, Cupo RR, Gao E, Csordás G, Slovinsky WS, Paillard M, et al. Mitochondrial fusion dynamics is robust in the heart and depends on calcium oscillations and contractile activity. Proc Natl Acad Sci U S A. 2017 Jan 31;114(5):E859–68.

41. Valente AJ, Maddalena LA, Robb EL, Moradi F, Stuart JA. A simple ImageJ macro tool for analyzing mitochondrial network morphology in mammalian cell culture. Acta Histochem. 2017 Apr 1;119(3):315–26.

42. Gao J, Shi X, He H, Zhang J, Lin D, Fu G, et al. Assessment of sarcoplasmic reticulum calcium reserve and intracellular diastolic calcium removal in isolated ventricular cardiomyocytes. Journal of Visualized Experiments. 2017 Sep 18;2017(127).
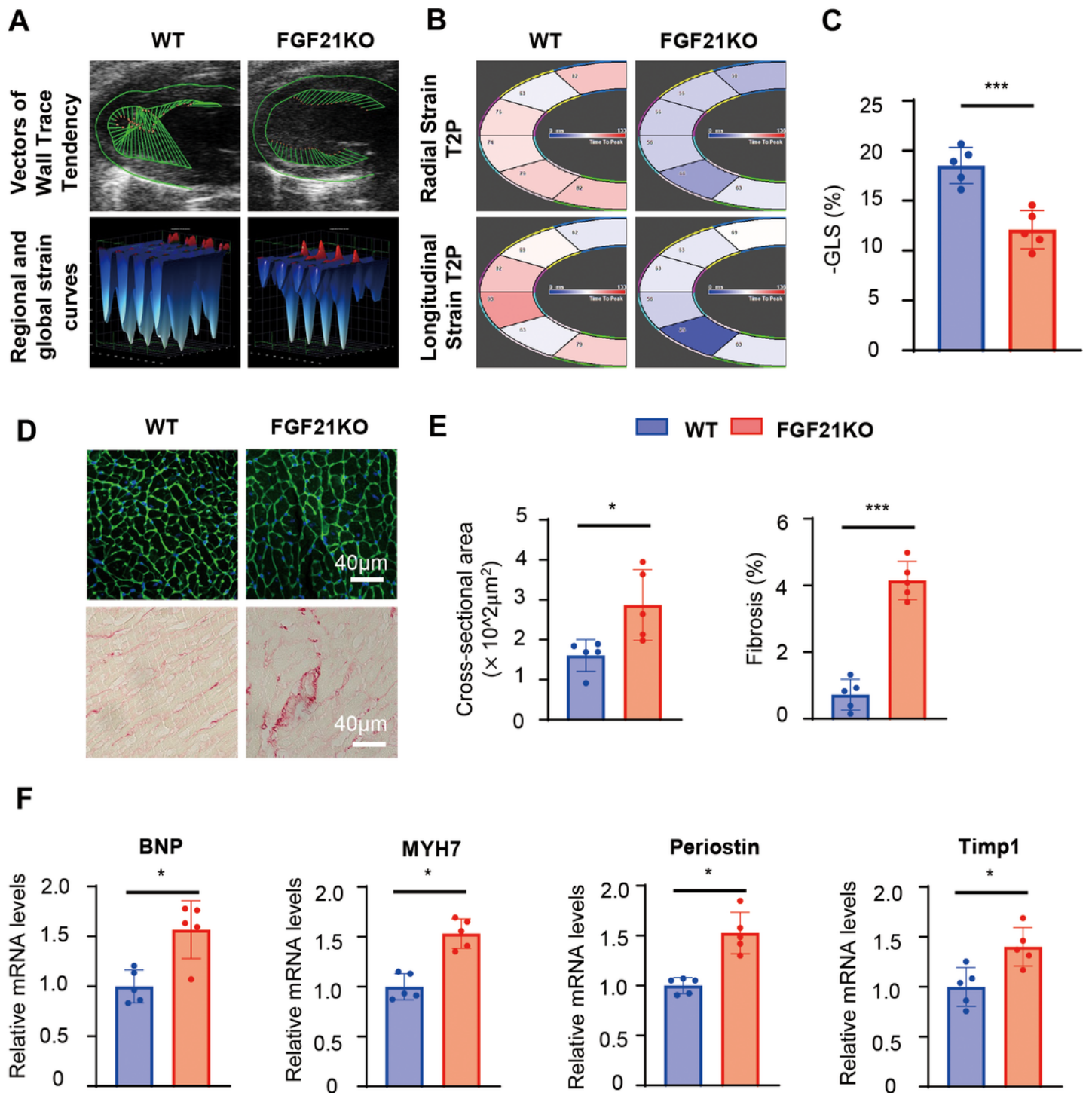
Figures

Figure 1

Figure 1

16-week FGF21 KO mice developed diastolic dysfunction, mild cardiac hypertrophy, and fibrosis

(A) Representative echocardiography images of vectors of wall trace tendency calculated by Vevo Software. (B) Representative echocardiography images of vectors of radial and longitudinal strain calculated by Vevo Software. (C) Left ventricular global longitudinal strain (GLS) was calculated by Vevo

Software. (D) Representative cross-sections of heart stained for WGA, and Sirius red in 16-week WT and FGF21 KO mice heart tissue. (E) Quantitative analysis of cardiomyocyte size (WGA staining), fibrotic area (red area in Sirius red staining). (F) qPCR analysis of mRNA expression levels of hypertrophic and fibrotic genes in the heart. (Representative data from three independent experiments are shown and presented as mean ± SD. *p< 0.05, **p< 0.01, ***p< 0.001. n=5 mice/group)
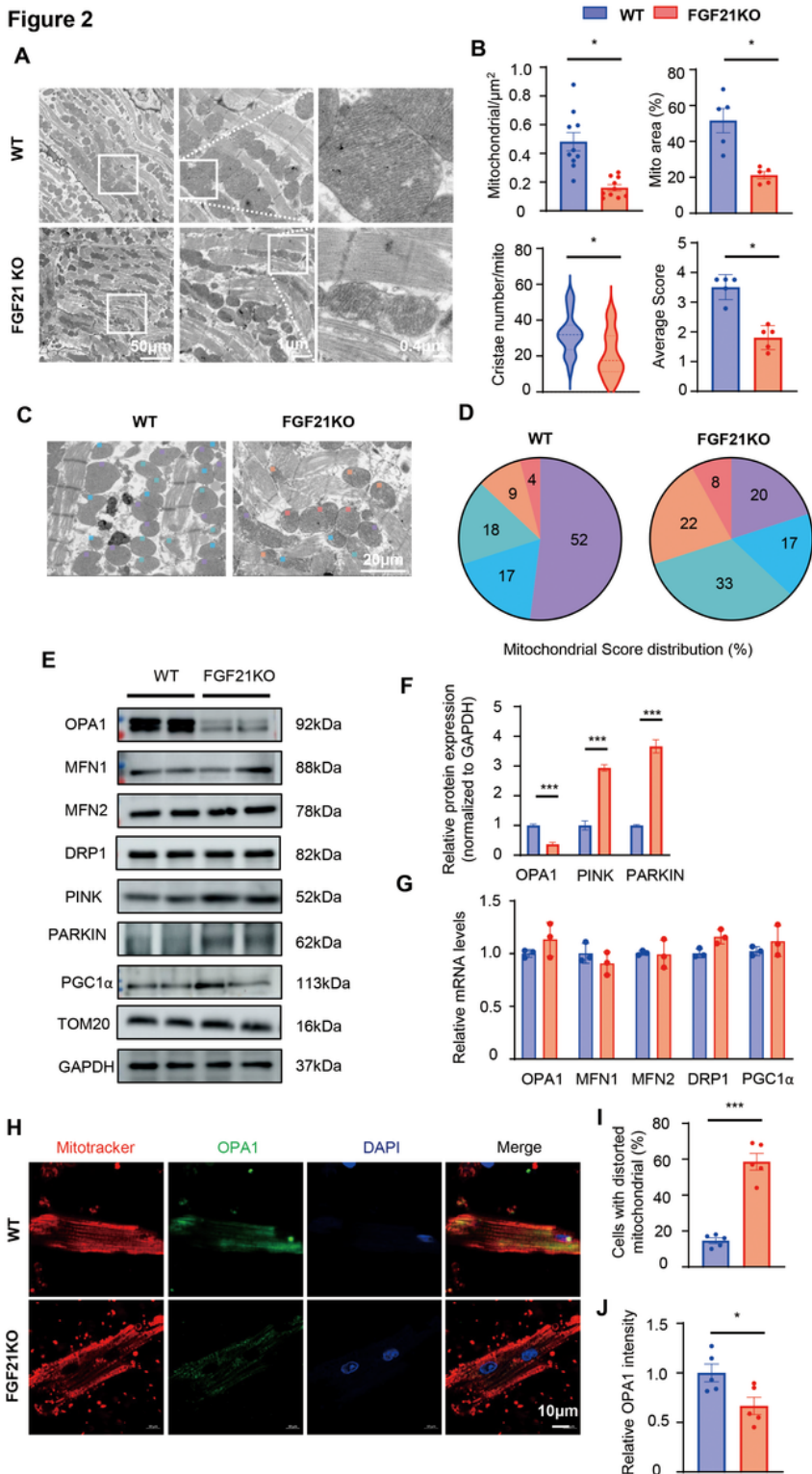
Figure 2

In FGF21 KO mice, mitochondrial morphology and functions are severely damaged.

(A) Representative electron microscopic (EM) images of heart sections. Per heart, 15 to 20 random fields were analyzed. (B) Quantification of number of mitochondrial, average mitochondria cross-sectional area, cristae number and mitochondria score. (C) Representative EM images of heart sections marked by a 5-grade scoring system. (D) Pie chart depicts the prevalence of the individual score grades across the analyzed mitochondrial population in each group. A total of 100 mitochondria in each sample were randomly analyzed. (E-F) Representatives immunoblot images of total proteins extracted from the heart tissues and quantified by densitometric analysis. (G) Relative mRNA levels of the mitochondrial dynamic related protein and mitochondrial genesis protein in the heart of 16-week WT and FGF21 KO mice. (H-J) Representative confocal images and quantification of isolated adult cardiomyocytes MitoTracker and OPA1 staining. (Representative data from three independent experiments are shown and presented as mean ± SD. *p< 0.05, **p< 0.01, ***p< 0.001. n=5 mice/group)
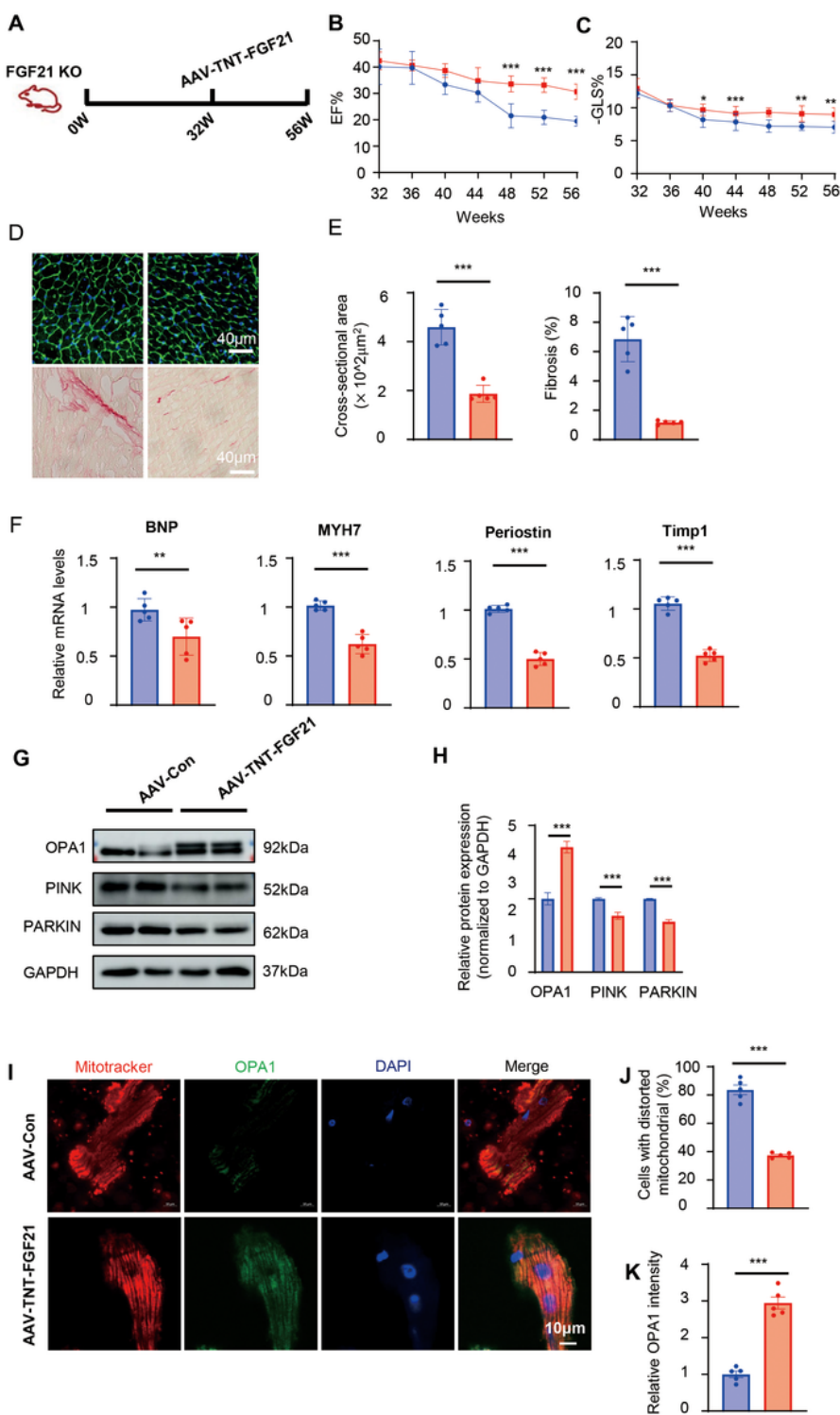
Figure 3

Cardiac specific overexpression of FGF21 could restore cardiac function in FGF21 KO mice

(A) 32-week-old male FGF21 KO mice and their wild-type littermates were given AAV-TNT-FGF21-GFP and AAV-TNT-GFP, then noninvasive echocardiographic assessments were performed to monitor cardiac function for 24 weeks. (B) Ejection fraction was measured by echocardiography every 4 weeks in AAV-

Con and AAV-TNT-FGF21 mice. (C) Left ventricular global longitudinal strain (GLS) was calculated by Vevo Software every 4 weeks. (D) Representative cross-sections of heart stained for WGA, and Sirius red in 16-week WT and FGF21 KO mice heart tissue. (E) Quantitative analysis of cardiomyocyte size (WGA staining), fibrotic area (red area in Sirius red staining). (F) qPCR analysis of mRNA expression levels of hypertrophic and fibrotic genes in the heart. (G-H) Representatives immunoblot images of total proteins extracted from the heart tissues and quantified by densitometric analysis. (I-K) Representative confocal images and quantification of isolated adult cardiomyocytes MitoTracker and OPA1 staining. (Representative data from three independent experiments are shown and presented as mean ± SD. *p< 0.05, **p< 0.01, ***p< 0.001, n=5 mice/group)
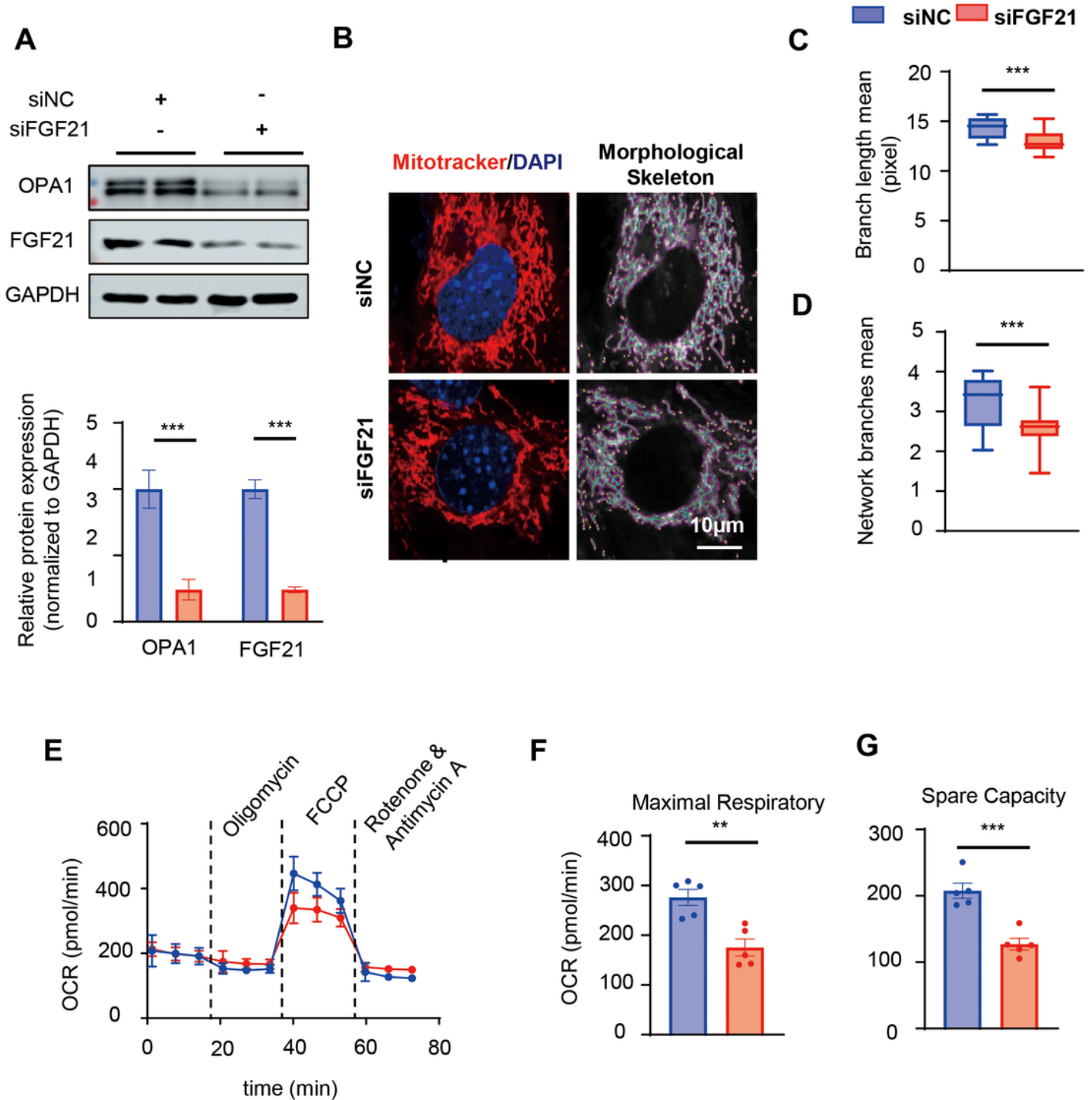
Figure 4

Figure 4

FGF21 knock down cardiomyocytes had abnormal mitochondrial structure and function

(A) Representatives immunoblot images to detect OPA1 after siFGF21 in cardiomyocytes. (B-D) FGF21 knock down cardiomyocyte damaged mitochondrial dynamics with decreased mitochondrial network branches and branch length. (E) Representative oxygen consumption curves in the siFGF21 and siNC

treated cardiomyocytes. Basal respiration rate was measured followed by proton leak after the addition of oligomycin, maximal respiration after the addition of FCCP, and non-mitochondrial respiration after the addition of rotenone. (F-G) Quantification analysis of maximal respiratory and spare capacity. (Representative data from three independent experiments are shown and presented as mean ± SD. *p< 0.05, **p< 0.01, ***p< 0.001)
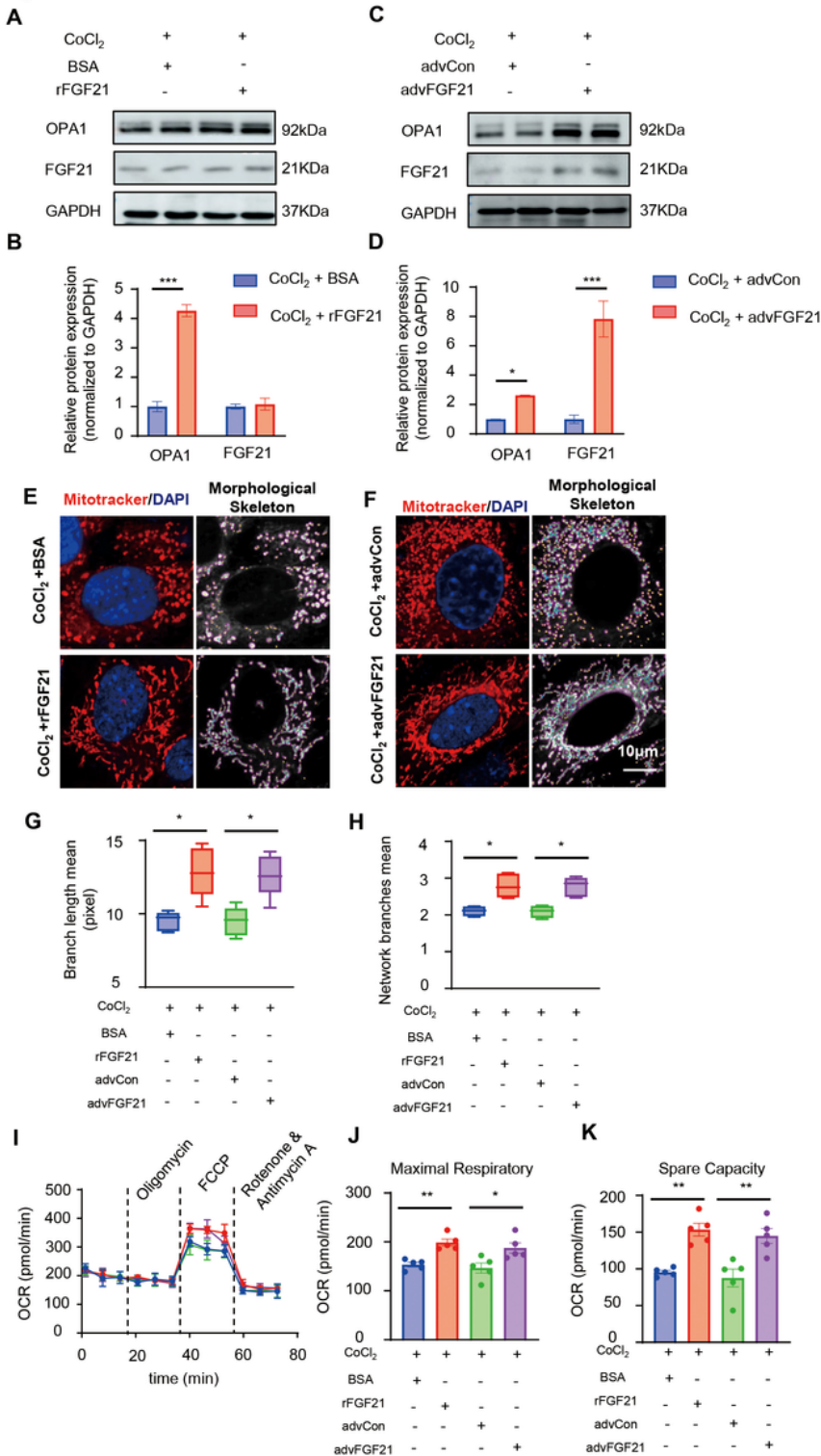
Figure 5

Figure 5

Both rFGF21 and advFGF21 could protect mitochondrial structure and function damage caused by CoCl$_2$.

(A-D) Representatives immunoblot images to detect OPA1 in rFGF21 and advFGF21 treated cardiomyocytes then treated with CoCl$_2$ (200nm) for 24h. (E-H) Mitochondrial dynamics detected with MitoTracker staining. In rFGF21 and advFGF21 treated cardiomyocytes then treated with CoCl$_2$ (200nm) for 24h, mitochondrial network branches and branch length. (I) Representative oxygen consumption curves in rFGF21 and advFGF21 treated cardiomyocytes then treated with CoCl$_2$ (200nm) for 24h. Basal respiration rate was measured followed by proton leak after the addition of oligomycin, maximal respiration after the addition of FCCP, and non-mitochondrial respiration after the addition of rotenone. (J, K) Quantification analysis of maximal respiratory and spare capacity. (Representative data from three independent experiments are shown and presented as mean ± SD. *p< 0.05, **p< 0.01, ***p< 0.001)
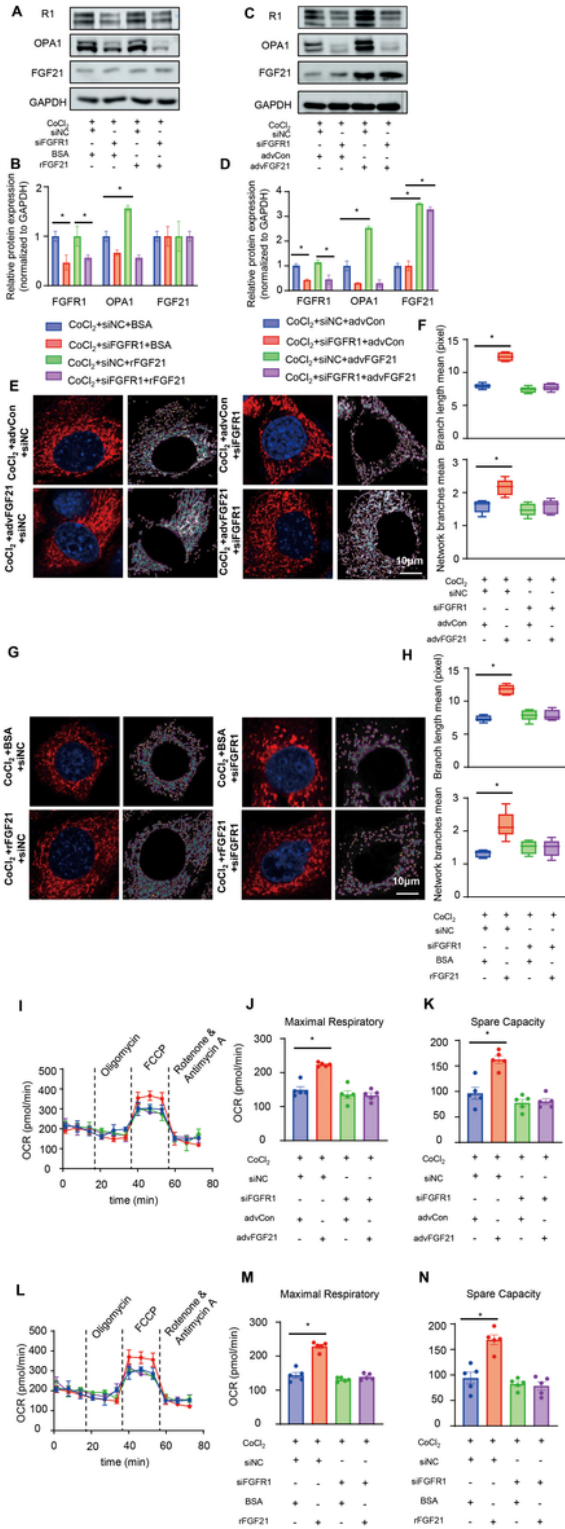
Figure 6

Knocked down FGFR1 impair the rFGF21 and advFGF21 mitochondria protection cause by CoCl$_2$.

(A-D) Representatives immunoblot images to detect OPA1 in siFGFR1 and siNC treated cardiomyocytes and transfected with rFGF21 or advFGF21 then treated with CoCl$_2$ (200nm) for 24h. (E-H) Mitochondrial dynamics detected with MitoTracker staining. In siFGFR1 and siNC treated cardiomyocytes and

transfected with rFGF21 or advFGF21 then treated with CoCl$_2$ (200nm) for 24h, mitochondrial network branches and branch length. (I, L) Representative oxygen consumption curves in siFGFR1 and siNC treated cardiomyocytes and transfected with rFGF21 or advFGF21 then treated with CoCl$_2$ (200nm) for 24h. Basal respiration rate was measured followed by proton leak after the addition of oligomycin, maximal respiration after the addition of FCCP, and non-mitochondrial respiration after the addition of rotenone. (J, K, M, N) Quantification analysis of maximal respiratory and spare capacity. (Representative data from three independent experiments are shown and presented as mean ± SD. *p< 0.05, **p< 0.01, ***p< 0.001)
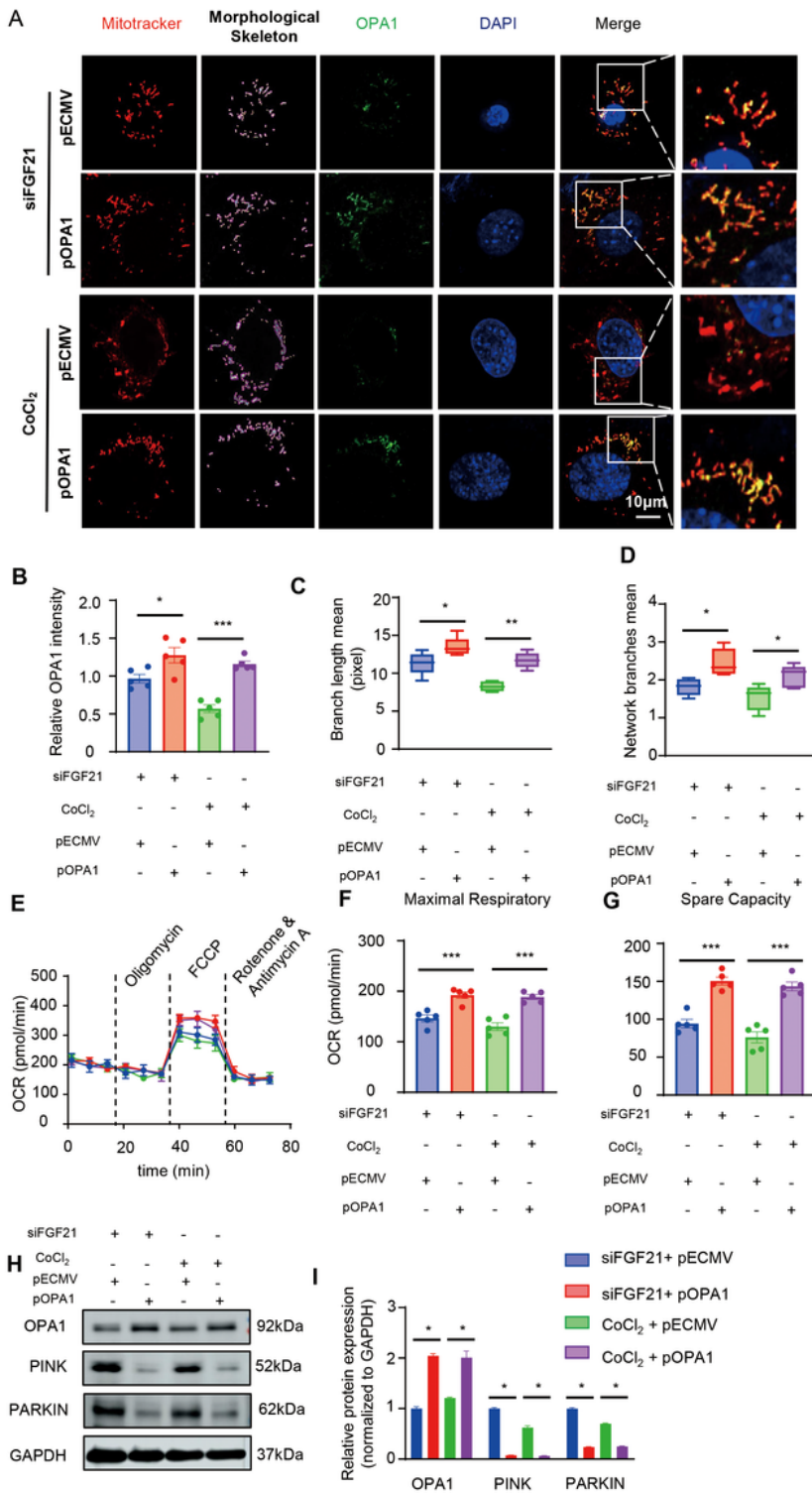
Figure 7

Figure 7

Overexpression of OPA1 restore the excess mitochondrial fission caused by FGF21 deficiency or under CoCl$_2$ stimulation

(A-B) Representative confocal images and quantification of MitoTracker and OPA1 staining of siFGF21 cardiomyocytes then transfect pOPA1 and cardiomyocytes transfected pOPA1 then treated with CoCl$_2$

(200nm) for 24h. (C-D) Quantification of mitochondrial network branches and branch length. (E) Representative oxygen consumption curves in siFGFR1 and siNC treated cardiomyocytes and transfected with advFGF21 and advCon then treated with $CoCl_2$ (200nm) for 24h. Basal respiration rate was measured followed by proton leak after the addition of oligomycin, maximal respiration after the addition of FCCP, and non-mitochondrial respiration after the addition of rotenone. (F-G) Quantification analysis of maximal respiratory and spare capacity. (H) Representatives immunoblot images to detect relative protein in siFGF21 and $CoCl_2$ treated cardiomyocytes and transfected with pOPA1 and pECMV. (Representative data from three independent experiments are shown and presented as mean ± SD. *p< 0.05, **p< 0.01, ***p< 0.001)
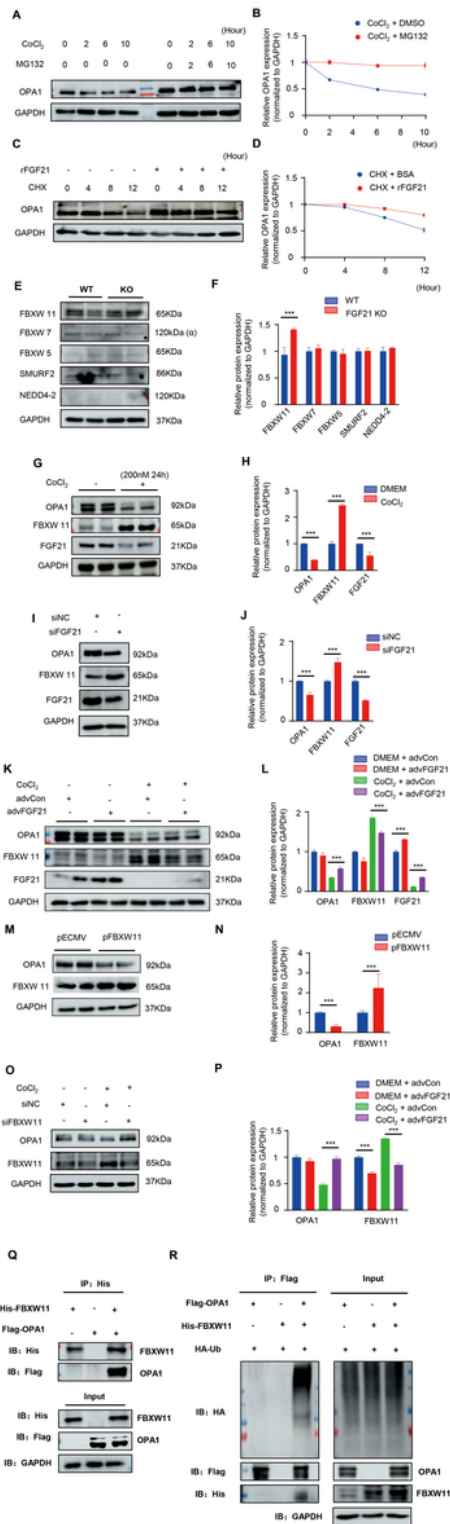
Figure 8

Figure 8

FBXW11 mediated FGF21 regulation of OPA1 degradation

(A, B) Representatives immunoblot images to detect OPA1 showed cardiomyocytes treated with MG132 could inhibited OPA1 degradation after treated with $CoCl_2$. (C, D) Representatives immunoblot images to detect OPA1 showed cardiomyocytes treated with CHX (20μg/ml) then given rFGF21 (50ng/ml) could

inhibited OPA1 degradation (E, F) Western blots showing the predicted OPA1 E3 ligase expression levels in FGF21 KO mice heart tissue. (G-J) In cardiomyocytes treated with $CoCl_2$ and in FGF21 knocked down cardiomyocytes FBXW11 decreased, (K-L) Western blots showing overexpression of FGF21 in cardiomyocytes could down regulated FBXW11. (M-P) Overexpression FBXW11 could decrease OPA1 levels and knocking down FBXW11 could increase OPA1 levels under $CoCl_2$ stimulation. (Q-R) IP analysis showed that FBXW11 could interacted with OPA1 and increased OPA1 ubiquitination. (Representative data from three independent experiments are shown and presented as mean ± SD. *p< 0.05, **p< 0.01, ***p< 0.001)

Supplementary Files

This is a list of supplementary files associated with this preprint. Click to download.

- SupplementaryInformation.pdf